# Investigating the particle to fibre transition threshold during electrohydrodynamic atomization of a polymer solution

O. Husain, W. Lau, M. Edirisinghe, M. Parhizkar *

Department of Mechanical Engineering, University College London, London, UK

ABSTRACT

Electrohydrodynamic atomization (EHDA) is a key research area for producing micro and nano-sized structures. This process can be categorized into two main operating regimes: electrospraying for particle generation and electrospinning for fibre production. Producing particles/fibres of the desired size or morphology depends on two main factors; properties of the polymeric solution used and the processing conditions including flow rate, applied voltage and collection distance. In this work the particle-fibre transition region was analyzed by changing the polymer concentration of PLGA poly (lactic-*co*-glycolic acid) in acetone between 2 and 25 wt%. Subsequently the processing conditions were adjusted to study the optimum transition parameters. Additionally the EHDA configuration was also modified by adding a metallic plate to observe the deposition area. The diameter and the distance of the plate from the capillary tip were adjusted to investigate variations in particle and fibre morphologies as well. It was found that complete transition from particles to fibres occurs at 20 wt% indicating concentration to be the dominant criterion. Low flow rates yielded fibres without beads. However the applied voltage and distance between the tip of the nozzle jetting the polymer solution and collector (working distance) did not yield definitive results. Reducing the collector distance and increasing applied voltages produces smooth as well as beaded fibres. Addition of a metal plate reduces particle size by ~1 μm; the fibre size increases especially with increasing plate diameter while bead density and size reduces when the disc is fixed closer to the capillary tip. Additionally, the deposition area is reduced by 70% and 57% with the addition of metal plates of 30 mm and 60 mm, respectively. The results indicate that a metal plate can be utilized further to tune the particle/fibre size and morphology and this also significantly increases the yield of EHDA process which is currently a limitation in adopting it as a mass production technique.

© 2016 The Authors. Published by Elsevier B.V. This is an open access article under the CC BY license (http://creativecommons.org/licenses/by/4.0/).

## 1. Introduction

Polymeric particles and fibres are finding uses in a range of industries from drug delivery and tissue engineering to food additives and even textiles [1]. A range of techniques exist for the production of these structures including spray drying and emulsion evaporation for particles [2] and thermal induced phase evaporation and self-assembly for fibres [3,4]. Included along with these processes is also the electrohydrodynamic atomization (EHDA) technique which as the name suggests is principally governed by electro-mechanical and hydrodynamic forces.

EHDA has been the subject of wide research for more than a century with several of its benefits being realized. It is well accepted that this process is suitable in terms of providing a well-controlled size and morphology [5,6] which is increasingly becoming a requirement for better efficiency. For example in the case of tissue engineering, electrospun collagen scaffolds possesses more homogeneous pore structures as opposed to freeze dried scaffolds [7]. Similarly electrospraying offers several advantages such as higher drug loading efficiency and narrower particle size distribution over other particle fabrication processes [8]. Electrospraying and electrospinning are two main electrohydrodynamic atomization techniques. Fibres via electrospinning and particles via electrospraying can be produced through proper selection of the processing parameters and solution properties. The basic difference between these two processes lies mainly in the concentration of the solutions [9]. In electrospraying, low viscosity solutions are used, as the concentration is sufficiently low to destabilize the electrified jet that breaks down into small droplets that further solidify through rapid evaporation process and form particles. In electrospinning, more viscous solutions with higher polymer concentration are used to form the charged jet, which after an initial straight path, undergoes "bending instability" and characteristic "whipping motion", and as a result fibres are formed [10].

Additionally, EHDA has proven to be a cost effective technology [11, 12] and one of the main advantages of this process is the wide range of materials that can be processed from solutions and also melts, emulsions etc. [4,13]. There has been a significant amount of interest in recent years in developing new printing methods for patterning

* Corresponding author.
E-mail address: maryam.parhizkar.09@ucl.ac.uk (M. Parhizkar).

**Table 1**
Properties of the PLGA solutions used in this work.

| PLGA concentration (wt%) | Density (kg/m$^3$) | Viscosity (mPa s) | Surface Tension (mN/m) | Electrical Conductivity (μS/m) |
|---|---|---|---|---|
| 2 | 770 | 0.63 ± 0.01 | 21.0 ± 0.1 | 319 ± 2 |
| 4 | 785 | 0.77 ± 0.01 | 22.3 ± 0.2 | 545 ± 6 |
| 10 | 801 | 1.74 ± 0.02 | 23.0 ± 0.2 | 255 ± 2 |
| 15 | 822 | 3.01 ± 0.02 | 24.4 ± 0.6 | 253 ± 3 |
| 20 | 846 | 7.68 ± 0.07 | 25.6 ± 0.4 | 229 ± 2 |
| 25 | 875 | 15.38 ± 0.22 | 32.1 ± 0.5 | 132 ± 5 |

materials in nano-scale [14,15]. EHD printing has many unique features such as formation of 3D products with high resolutions and the ability of using coarser nozzles in order to avoid clogging [16].

This study derives its need from the current limitation EHDA faces in terms of reproducibility and accuracy [17]. The overall process is dependent on multiple aspects, all of which have an interdependent relationship further complicating the dynamics of EHDA. As a result this proves to be a major hurdle in upscaling the process to an industrial level where consistency would be necessary for mass production. As a result, EHDA has become a flourishing research area for micro/nanolevel particle and fibre production [18].

The main aim of this work was to define the effects of the parameters on which the particle and fibre formation process is based in electrohydrodynamic processing. Primarily this included the effect of solution parameters in terms of concentration and the process parameters, specifically flow rate, applied voltage and nozzle tip-collector distance. Additionally, another area investigated within the scope of this work was the effect of an auxiliary metal plate. The main aim was to comprehend whether this EHDA set-up modification induced any changes in relation to the produced particle/fibre morphology.

Transition from particle to fibre formation has a high correlation with respect to the polymer concentration in the solution. Quantitatively this transition process for different polymeric solutions has been characterized using the Berry number [19] which is a product of the intrinsic viscosity and the solution concentration as described in Eq. 1.

$$B_e = [\eta]C \quad (1)$$

where $B_e$ is the Berry number, $([\eta] = \lim_{c \to 0} \eta_{red})$ is the intrinsic viscosity, which is calculated by determining the reduced viscosity ($\eta_{red} = \frac{\eta_{sp}}{C}$,

where $\eta_{sp}$ is the specific viscosity) and extrapolating to infinite dilution, and $C$ is the polymer concentration.

The Berry number has a quantitative significance as it maps out the transition regime between electrospraying and electrospinning. As a result different regions have been mapped out as summarized in Eq. 2.

$$B_e = \begin{cases} <1 \ (C<C^*) \\ <4 \ (C^*<C<C_e) \\ >4 \ (C>C_e) \end{cases} \quad (2)$$

$$C^* = 1/[\eta] \quad (3)$$

where $C$ is the polymer concentration, $C^*$ is the critical overlap concentration and $C_e$ is the chain entanglement concentration. The first region is defined as the dilute region up to the point where $B_e \sim 1$, and the working polymer concentration is $<C^*$ as defined in Eq. 3. Here, the intermolecular entanglement is significantly weak, limiting viscous effects, resulting in electrospraying. This transition phenomenon can be further subdivided into different regimes, the first being the semi dilute unentangled regime where increasing concentration leads to significant chain overlap. The $B_e$ values in this region correspond to $1 < B_e < 4$. However the chain overlapping/polymer–polymer interaction does not prove to be sufficient enough to inhibit molecular motion due to which the occurrence of particles, and as a result beaded and non-continuous fibres are common.

Beyond values of $B_e > 4$, researchers [19–21] have generally observed the formation of pure fibres completing the transition to what is termed as the semi-dilute entangled regime. Specifically, in terms of concentration, this transition is signified by $C_e$. Hong et al. [21] observed a steep rise in viscosity at $B_e > 5$ resulting in a strong chain overlap. Because of this the chain entanglement proves to be competent enough to hinder
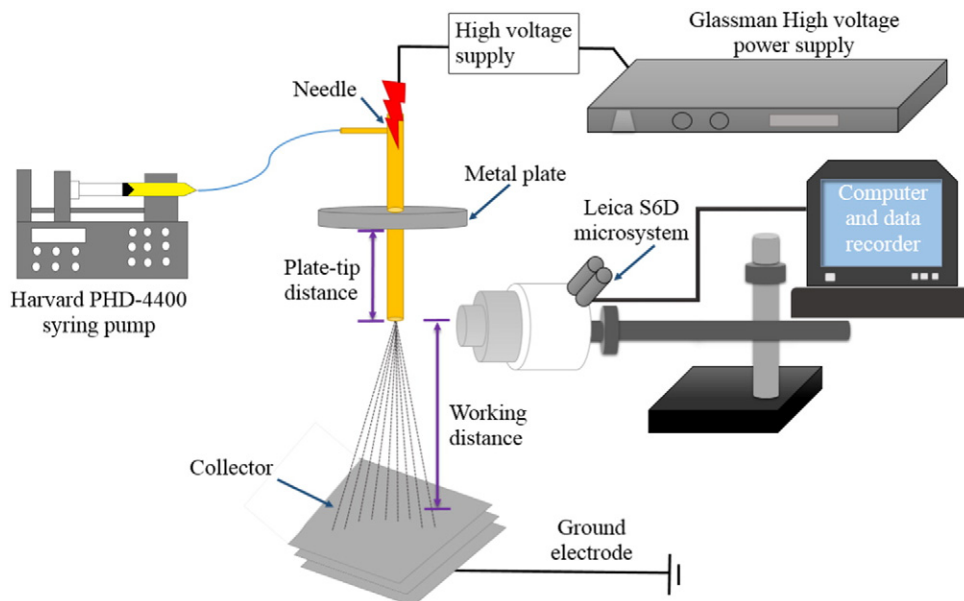


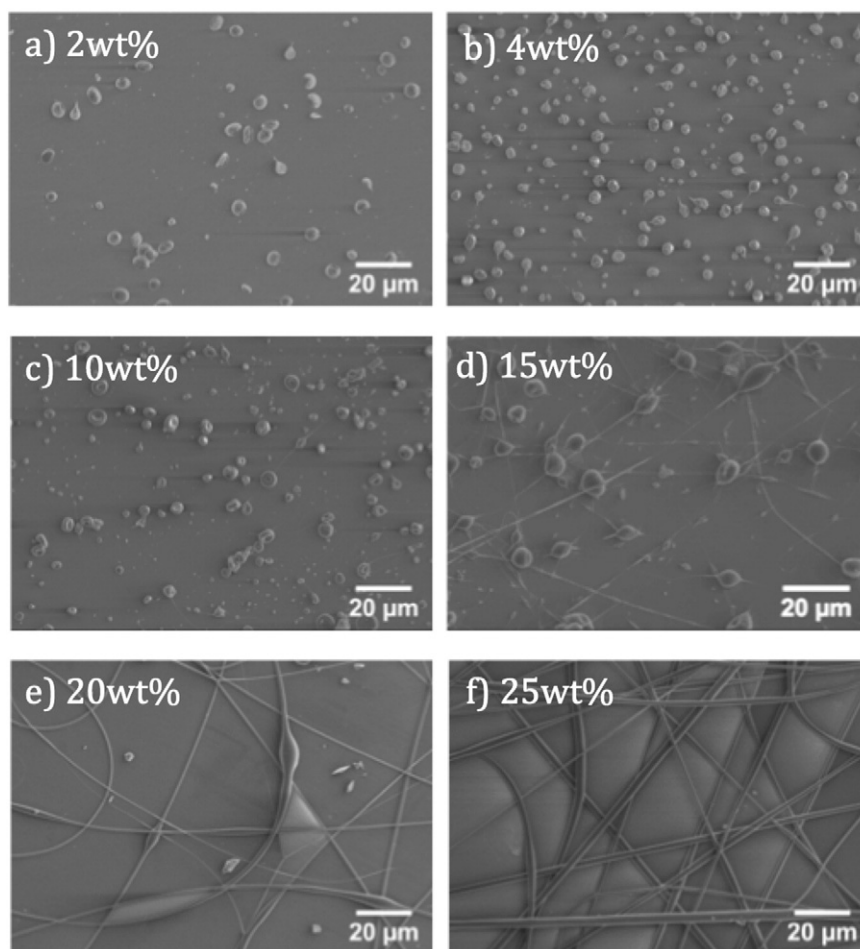**Fig. 1.** Schematic illustration of the EHDA apparatus used in this work.

**Fig. 2.** Scanning electron micrographs of EHDA products obtained (the flow rate, applied voltage and working distance tested were 50 μL/min, 15 kV and 200 mm, respectively).

molecular motion and ultimately the visco-elastic stresses are strong enough to prevent fibre fracture.

## 2. Experimental details

### 2.1. Materials and solution characterization

All the experiments were carried out with PLGA (*co*-polymer 50:50, Resomer RG503H, molecular weight: 33,000 g mol$^{-1}$) which was purchased from Boehringer (Ingelheim, Germany). PLGA is an FDA approved polymer and is widely used for biomedical applications. Acetone (from Sigma-Aldrich, Poole, UK) was used as the solvent due to its non-toxic nature. PLGA solutions of the required concentrations were prepared by mixing appropriate amounts of polymer and solvent. All the solutions were formulated at a fixed solution volume of 20 mL. To ensure a homogeneous mix, each solution was magnetically stirred for a minimum period of 300 s. Table 1 describes the different solutions prepared during the course of the experiments.

Viscosity, surface tension, density and electrical conductivity of all the prepared solutions were characterized. Density was measured using a standard density bottle DIN ISO 3507-Gay-Lussac. Viscosity measurements were conducted using a U-tube viscometer (size E, VWR, UK). Prior to measurements the viscometer was calibrated and checked with ethanol to remove any residual particles. A Kruss tensiometer (Model DSA100, Kruss GmbH, Hamburg, Germany) was used to measure the surface tension using the Wilhelmy's plate method. Electrical conductivity of each solution prepared was estimated using a conductivity probe (Jenway 3540pH/conductivity meter). All the measurements, presented in Table 1, were conducted at the ambient

temperature (21 °C) and relative humidity of 40–50% after calibrating the equipment with distilled water.

### 2.2. Particle/fibre characterization

All the samples were collected on glass microscope slides. These were analyzed mainly under an optical microscope (Nikon Eclipse ME 600) fitted with a camera (Micropublisher 3.3 RTV, 3.3megapixel CCD Color-Bayer Mosaic, Real Time Viewing camera, Media Cybernetics, Marlow, UK). This formed the basis to determine whether the samples require further analysis using scanning electron microscopy (SEM, Hitachi S-3400N) to investigate the morphology of the collected samples. The images obtained were analyzed further using *ImageJ* (National Institute of Health, USA) software to measure the particle, beads and fibre size (approximately 150–200 particles and 80–100 fibres were measured from different locations on the glass slides). The error bars in each graph indicate the standard deviation of the measurements carried out.

### 2.3. EHDA setup

Fig. 1 shows a schematic of the apparatus used. The EHD needle (17G, ID: 1.09 mm and OD: 1.50 mm) was connected to a syringe controlled by a syringe pump (PHD 4400, Harvard Apparatus Limited, Edenbridge, UK). The pump was used to control the flow rate through the needle. A high precision voltage generator (Glassman Europe Ltd., Bramley, UK) supplied the required electric field to the solution. In order to investigate the effect of the addition of the auxiliary plate on the particle/fibre formation and size, the EHDA setup was modified in
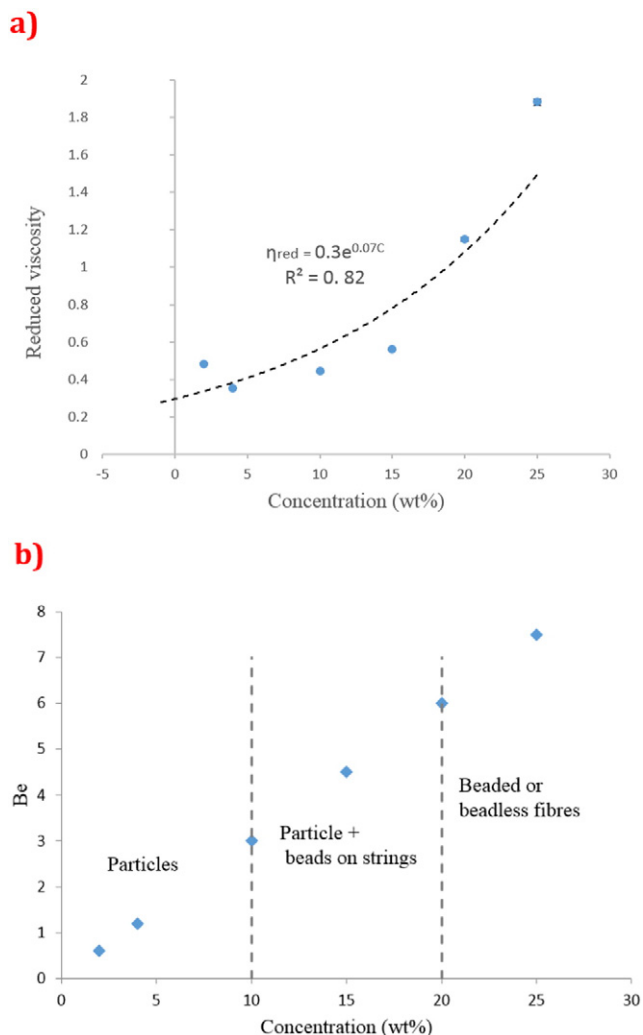
a)



b)



**Fig. 3.** a) Intrinsic viscosity of the solution used and b) Berry number-Morphology of products-Polymer concentration map.

some experiments by inserting metal plates of various size (30 mm and 60 mm in diameter). The plates were attached at two fixed distances of 5 mm and 25 mm from the capillary tip as shown in Fig. 1. All the experiments were conducted at the ambient temperature of 21 °C and relative humidity was controlled between 40 and 50%.

## 3. Results and discussion

### 3.1. Transition regime

Changing the concentration proved to be a clear differentiator between particle and fibre formation. Effects of concentration have been widely tested and characterized [22,23] and the results obtained in this work are in agreement with the general trends observed through the variation of concentration. At a lower concentration of 2 wt% (Fig. 2a) and 4 wt% (Fig. 2b) electrospraying was observed due to the solutions being unable to cause chain entanglement. The main competing forces comprised of the surface tension and the electrical conductivity both which contributed to the jet breakdown. As a result, obtaining a sustained jet yielding fibres was not possible.

While 10 wt% (Fig. 2c) appears to be a significant increase in concentration compared with 4 wt%, electrospraying was still the dominant phenomenon. This is expected since the measured viscosity shows a rise of approximately 1 mPa s which is still relatively small. Although the visco-elastic stresses are not strong enough, the rise in viscous

effects does have an effect on the morphological variation, mainly manifested by the formation of tailed particle structures. As the viscous effects become more significant at 3 mPa s at 15 wt%, the formation of particles and significant beads on string structures can also be seen (Fig. 2d). Simultaneously the observed increase in surface tension at higher concentrations shows that it is still strong enough to compete with the low visco-elastic stresses in generating particles and beads.

Beyond 15 wt% the viscosity rises steeply from 3 to 7 mPa s explaining the formation of only fibres at 20 wt% (Fig. 2e). The significant amount of chain entanglement and overlap at this concentration prevents jet fracture caused by the electrostatic field. Resistance offered by the visco-elastic stresses to the surface tension plays a key role in reducing the bead density. Qualitatively this is supported by the shape of beads which are more spindle-like, generally observed at higher viscosities [24].

As the viscosity further increases to 15 mPa s at 25 wt% (Fig. 2f), polymer chain interaction is quite high for the specific processing condition, leading to the formation of mostly smooth fibres. While a few beads are still observed, the beads are highly elongated relative to those seen at 20 wt%.

### 3.2. Quantification of the transition process

Prior to estimating the $B_e$, the values for the specific viscosity were extrapolated to estimate the intrinsic viscosity as shown in Fig. 3a. The $R^2$ value of the extrapolated trend line to zero concentration gives a value of 0.82 which appears to show a good fit with the actual data. As indicated in Fig. 3a, the intrinsic viscosity estimated for PLGA in acetone is approximately 0.3. This is in good agreement with the values that have been reported in literature [25]. The intrinsic viscosity is deemed to be an important variable as it could allow for further correlation with the degree to which a polymer forms inter- or intra-molecular chain entanglements at different concentrations [25].

Quantitative mapping of the transition mechanism in terms of the $B_e$ shows that $B_e > 6$ is required as indicated in Fig. 3b for complete fibre formation or in other words for the solution to enter the semi-dilute entangled region. For the specific polymer-solvent system utilized, this parameter has not been mapped before; $B_e$ values for other solution systems have been reported in literature [26–28]. The $B_e$ value estimated here appears to be in close correlation with the reported values. For example; $B_e > 4$ was necessary for uniform fibre formation in PAN/DMF solution [28]. Hsu and Shivkumar [27] observed $B_e > 4.5$ is needed for PCL in chloroform. Gupta et al. [19] electrospun PMMA in DMF, when $4 < B_e < 10$, while Koski et al. [28] obtained continuous fibre from PVA in aqueous solution at $5 < B_e < 9$ for different molecular weights of PVA.

It would be reasonable to expect variations in the reported values as the polymer concentration is just one factor which affects the particle/fibre formation process. For example, changing the molecular weight of the polymer can either increase or decrease the threshold for fibre formation by affecting the polymer-solvent interaction as observed by Koski et al. [28]. Similarly the type and solubility of the polymer in the solvent used would be another governing factor affecting the intrinsic viscosity.

One aspect where the estimated $B_e$ value for the PLGA-acetone system is in agreement with $B_e$ values of different solutions is the minimum threshold required for fibre formation. Obtaining complete fibres or even a fibre dominant morphology is highly unlikely at $B_e < 4$ and particles and beads on strings would be more prevalent.

### 3.3. Size distribution of particles and fibres

In the electrospraying regime (2–15 wt%) the particle size appears to be steadily increasing with concentration (Fig. 4a). The increase in concentration has raised the average particle size from $4.36 \pm 0.9$ μm at 2 wt% to $8.99 \pm 2.4$ μm at 15 wt%. Concentration also shows an effect on the particle size distribution. 2 wt% appears to have a narrower size
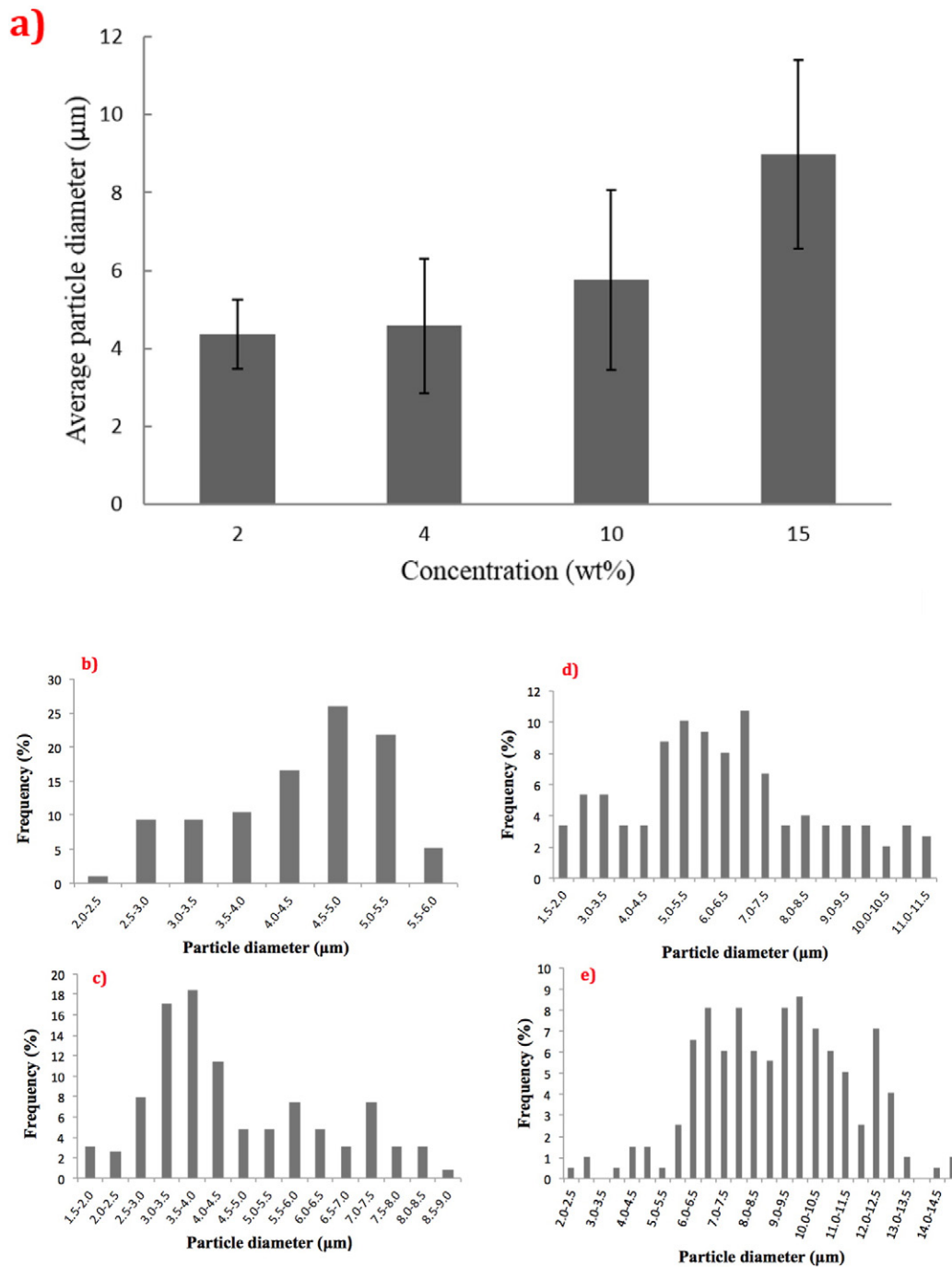
Fig. 4. a) Variation in particle size with polymer concentration and size distribution of particles at b) 2 wt%, c) 4 wt%, and d) 10 wt% and e) 15 wt% (the flow rate, applied voltage and working distance used were 50 μL/min, 15 kV and 200 mm, respectively).

distribution (Fig. 4b). The variation in particle size becomes more pronounced with increasing the concentration as can be observed from the size distribution graphs at 4 wt%, 10 wt% and 15 wt% (Fig. 4c, d and e, respectively).

For concentrations where electrospinning was observed (20 wt% and 25 wt%) a similar trend was noticeable. As observed from Fig. 5a, increasing the PLGA concentration from 20 wt% to 25 wt% resulted in an average fibre diameter increase from $1.78 \pm 0.4$ μm to $3.26 \pm 0.6$ μm. The size distribution of fibres (Fig. 5b and c) shows that in comparison, it is narrower at 20 wt% while at 25 wt% the distribution is much broader. Even the maximum fibre size is almost double of what is observed at 20 wt%. Fig. 6a and b show micrographs and variation of fibre size with applied voltage for a fixed flow rate of 50 μL/min at two

different working distances of 150 and 200 mm. As observed in Fig. 6a for both distances, the average fibre size decreased with the increase in applied voltage at 20 wt% concentration, however this trend was not found at the higher concentration of 25 wt% (Fig. 6b). At higher concentrations, the solvent/polymer ratio would be reduced and as the solvent evaporates from the droplet the increased concentration of PLGA would result in larger particle/fibre structures. Greater size variations observed at higher concentration on the other hand can be explained on the basis of the forces acting on the jet [29].

In electrospraying viscous effects are insignificant, leaving the surface tension and electrical conductivity as the main competing forces. Generally the surface tension would act to reduce the surface area of the jet promoting larger particle size [30]. The electric field on the
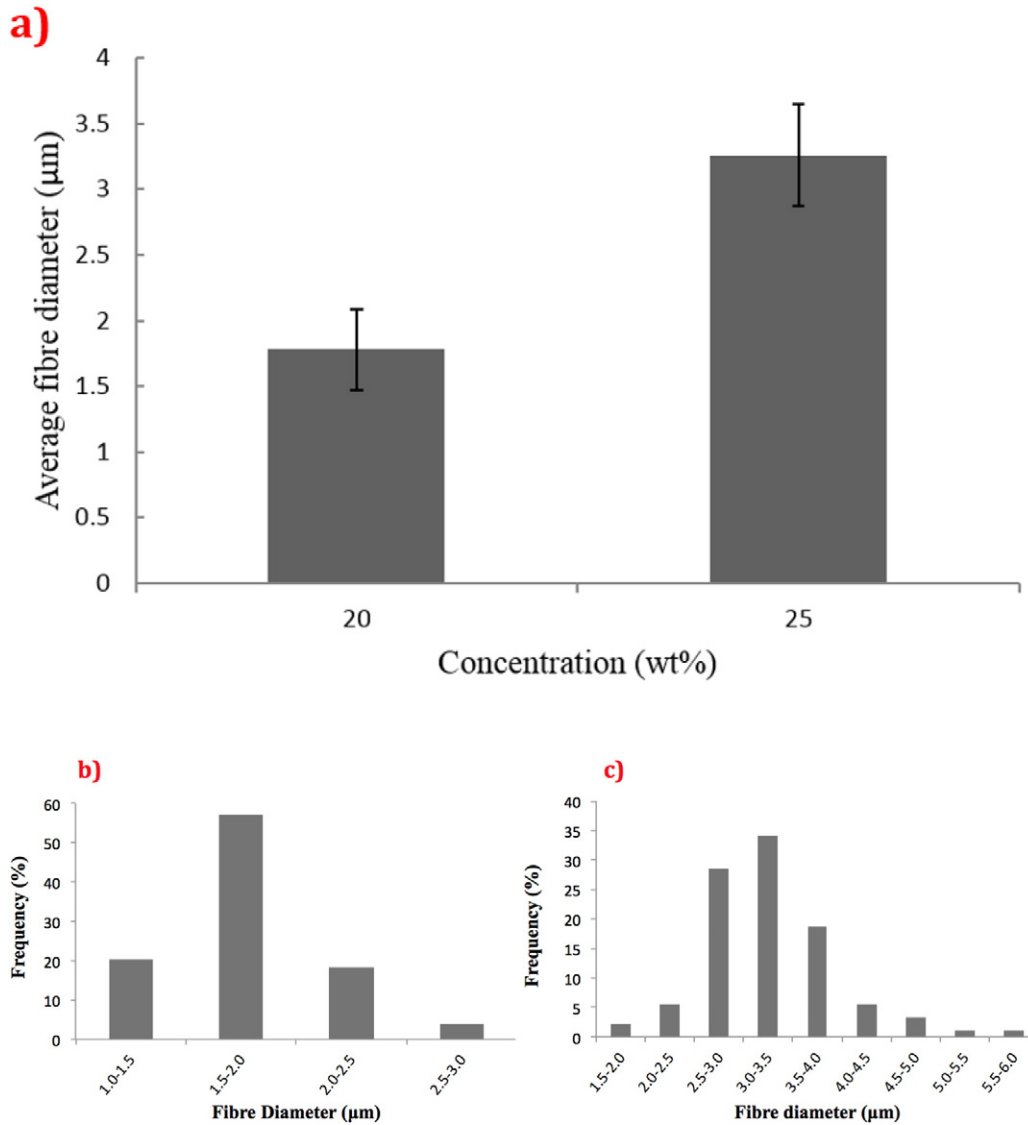
**Fig. 5.** a) Fibre size variation with polymer concentration and size distribution of fibres at b) 20 wt%, and c) 25 wt% polymer (the flow rate, applied voltage and working distance used were 50 μL/min, 15 kV and 200 mm, respectively).

other hand would induce greater charge repulsion increasing the surface area [31]. This charge repulsion is the main reason for the particle breakdown as it flows down on to the collector.

In electrospinning, visco-elastic stress resists any further change in fibre morphology. Apart from bead formation, surface tension has minor effects on the fibre size [32] but the electric field competes with the visco-elastic stress to promote tension within the fibres leading to fibre thinning. At 25 wt% the visco-elastic stress is relatively more dominant than at 20 wt% resulting in thicker fibres.

### 3.4. EHDA under an auxiliary metal plate

#### 3.4.1. Electrospraying

Optical microscopic images of particles electrosprayed with and without an auxiliary metal plate are shown in Fig. 7a with their corresponding size distribution. Electrospraying in the presence of a metal plate clearly shows a reduction in particle size as can be seen from Fig. 7b and the size distribution is narrower when making use of a metal plate at the different applied voltages tested. Additionally, it indicates that the frequency of obtaining particles <5 μm is much higher when electrospraying under the plate configuration.

#### 3.4.2. Electrospinning

Changing the system configuration showed significant variations in size and morphology of the fibres as well as the shape of the jet. Fibres electrospun without an auxiliary metal plate were highly beaded in nature (both for 20 and 25 wt% concentrations as Figs. 8a(i, ii) and 9a depict). For the 20 wt% concentration, the addition of both 30 mm and 60 mm diameter auxiliary plates placed at a distance of 5 mm above the needle tip resulted in smother fibres. On the other hand, increasing the plate-tip distance to 25 mm led to the generation of beaded fibres. Fig. 8b, demonstrates the variation of average fibre size with applied voltage at different plate-tip distances and different auxiliary plate diameter.

In the case of the average fibre size, for the 25 wt% concentration (Fig. 9a, b), configurations with a metal plate seem to have an effect on the fibre diameter which is generally smaller for the 60 mm metal plate compared to the fibres electrospun without an auxiliary metal plate. Further, from Fig. 9b it can be inferred that the 60 mm metal plate yields smaller diameter fibres in comparison with the 30 mm metal plate, irrespective of the plate-tip distance.

The increase in the average field strength in the presence of a plate as reported by Yang et al. [33] leads to greater bending speeds in the whipping instability region sufficiently stretching the fibres.
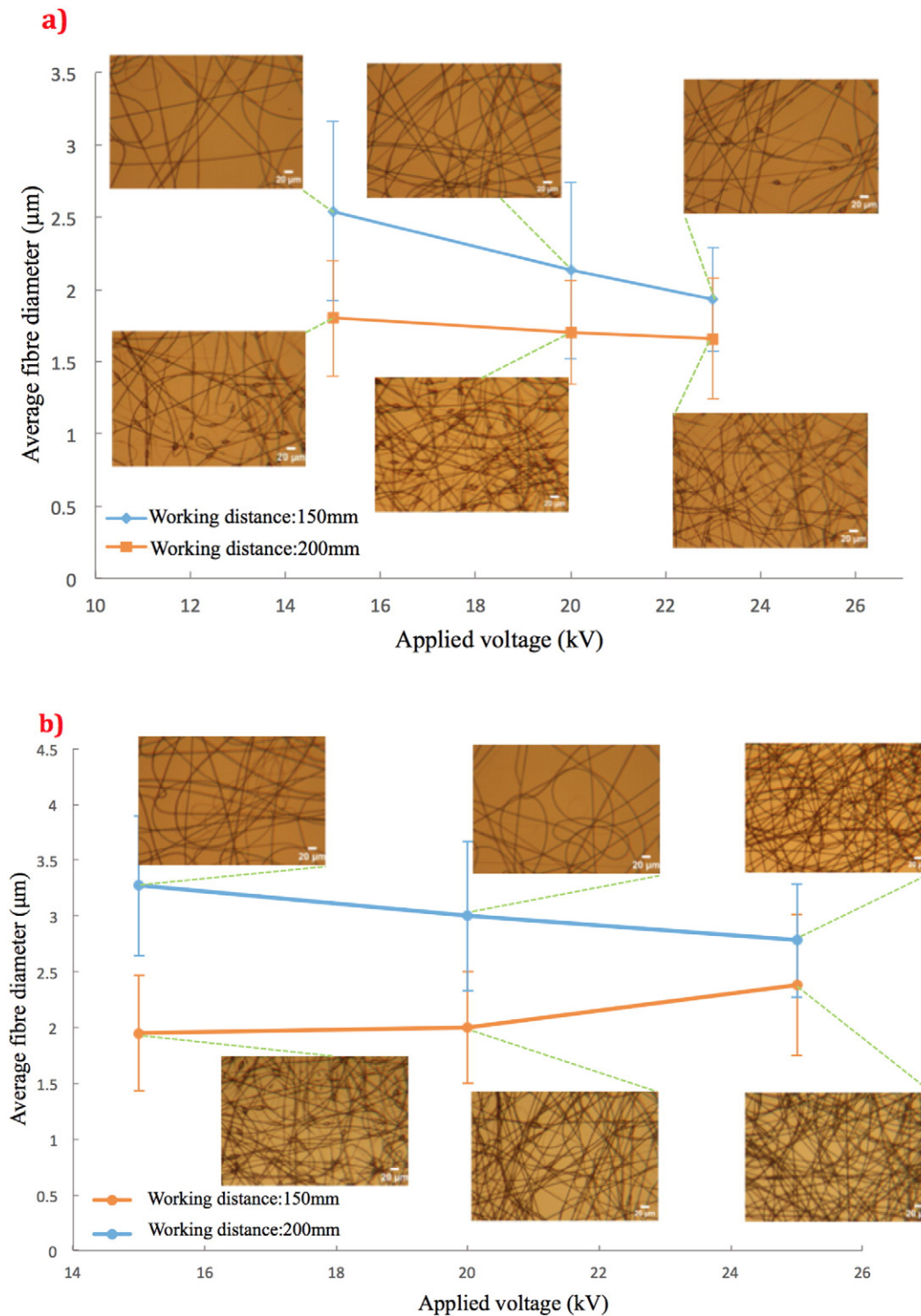
**a)**



**b)**



Fig. 6. Fibre size variation with applied voltage for solutions with a) 20 wt% and b) 25 wt% polymer concentration for a fixed flow rate of 50 μL/min at two different working distances of 150 and 200 mm (typical micrographs of products obtained are also shown).

As a result when both 30 and 60 mm plates were fixed at 5 mm from the tip of the nozzle, fibres were much smoother with reduced bead sizes.

At 25 mm however, the greater distance between the plate and the tip reduces the effect of the plate on the electric field and thus the uniformity, resulting in larger bead sizes. At both working distances the average bead size is greater for the 60 mm plate even if the bead density is reduced. This would be explainable on the basis of the larger cone jet, which is formed under the 60 mm plate.

The results also show that the effect of the plate does not appear to be limited along the working distance direction. In the absence of an auxiliary plate the electric field is highly focused in the vertical direction as opposed to the presence of the plate where the electric field is distributed in the horizontal plane as well, generating a uniform electric field gradient [34]. Following on from this argument, at a plate-tip distance of 25 mm using a smaller plate diameter of 30 mm is possibly less effective in distributing the electric field along the horizontal direction in comparison to the 60 mm plate. As a result the combined effect of the
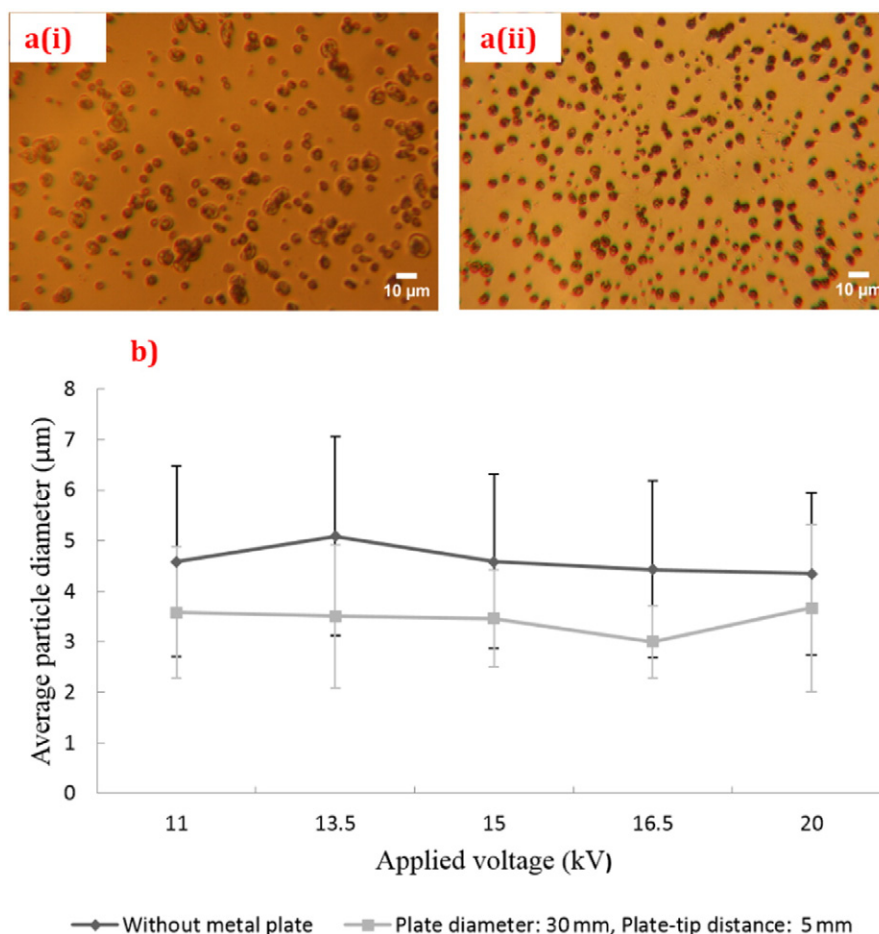
Fig. 7. Optical micrographs of EHDA products obtained at applied voltage of 15 kV a(i) without metal plate and a(ii) with 30 mm diameter metal plate and b) particle size variation of EHDA products generated without metal plate and with 30 mm diameter metal plate (the flow rate and working distance used were 50 μL/min and 200 mm, respectively).

reduced plate diameter when using the 30 mm plate and the increased plate-tip distance possibly does not increase the overall average electric field strength to a level necessary to reduce bead formation.

### 3.4.3. Collection area

As part of the experiments performed with the auxiliary metal plate, the collection area was also examined. Samples were collected at a working distance of 150 mm. While examining the collection area under both configurations, the fibres were electrospun for a time period of 120 s and collected on an aluminum foil.

Fig. 10 shows the collection of fibres under normal conditions as well as electrospinning performed in the presence of an auxiliary metal plate. The collection area of the fibres was further examined by using *ImageJ*. The deposition area is reduced by 70% using the 60 mm metal plate while by incorporating the 30 mm metal plate, the reduction is approximately 57% in the presence of the metal plate. A second advantage that a uniform electric field offers can be inferred from the reduced fibre deposition area. Under the plate the electric field is much more concentrated to a specific area and therefore allowing the fibres to be collected more efficiently. Potentially this is one manner through which yield can be increased which is currently a limitation in existing EHDA setups [35].

## 4. Conclusions

In this study the transition mechanism between formation of particles and fibres by EHDA was investigated by varying the solution properties and processing conditions. It was seen that transitions showed a primary dependency on the polymer concentration. Low polymer concentrations between 2 wt%–4 wt% resulted in electrospraying, while a mixture of particles and beads-on strings was dominant at intermediate concentrations of 10 wt% and 15 wt% at higher concentrations of 20 wt% and 25 wt%, only fibres were obtained. At higher concentrations the bead density reduced and the beads appeared more spindle shaped.

Smoother transition to uniform non-beaded fibres was facilitated by lower flow rates (e. g. higher flow rates produced beads with the shape gradually changing from spindle-like to spherical as the flow rate was increased).

Results on changing the working distance and applied voltage at different polymer concentrations were not in mutual agreement. Lower working distances and higher applied voltage produced smooth as well as beaded fibres. Furthermore even the average fibre size did not show any specific trend on changing these variables.

Further experiments were conducted by modifying the EHDA set-up with an auxiliary metal plate attached to the needle tip. A number of key changes were observed and some of the results obtained are distinct from the existing literature available on this type of modification. More precisely, particle diameter was found to be significantly reduced and a narrower size distribution was more prevalent. In electrospinning, the plate dimension and the distance of the plate from the capillary tip were observed to affect the morphological formation of fibres and their sizes. Beads in between fibres were reduced when the auxiliary plate was attached closer to the capillary tip. However, at large distances from the capillary tip, a minimum plate dimension was necessary to influence the formation of fibres without beads. Fibre diameter was found to be dependent primarily on the plate dimension with a larger plate
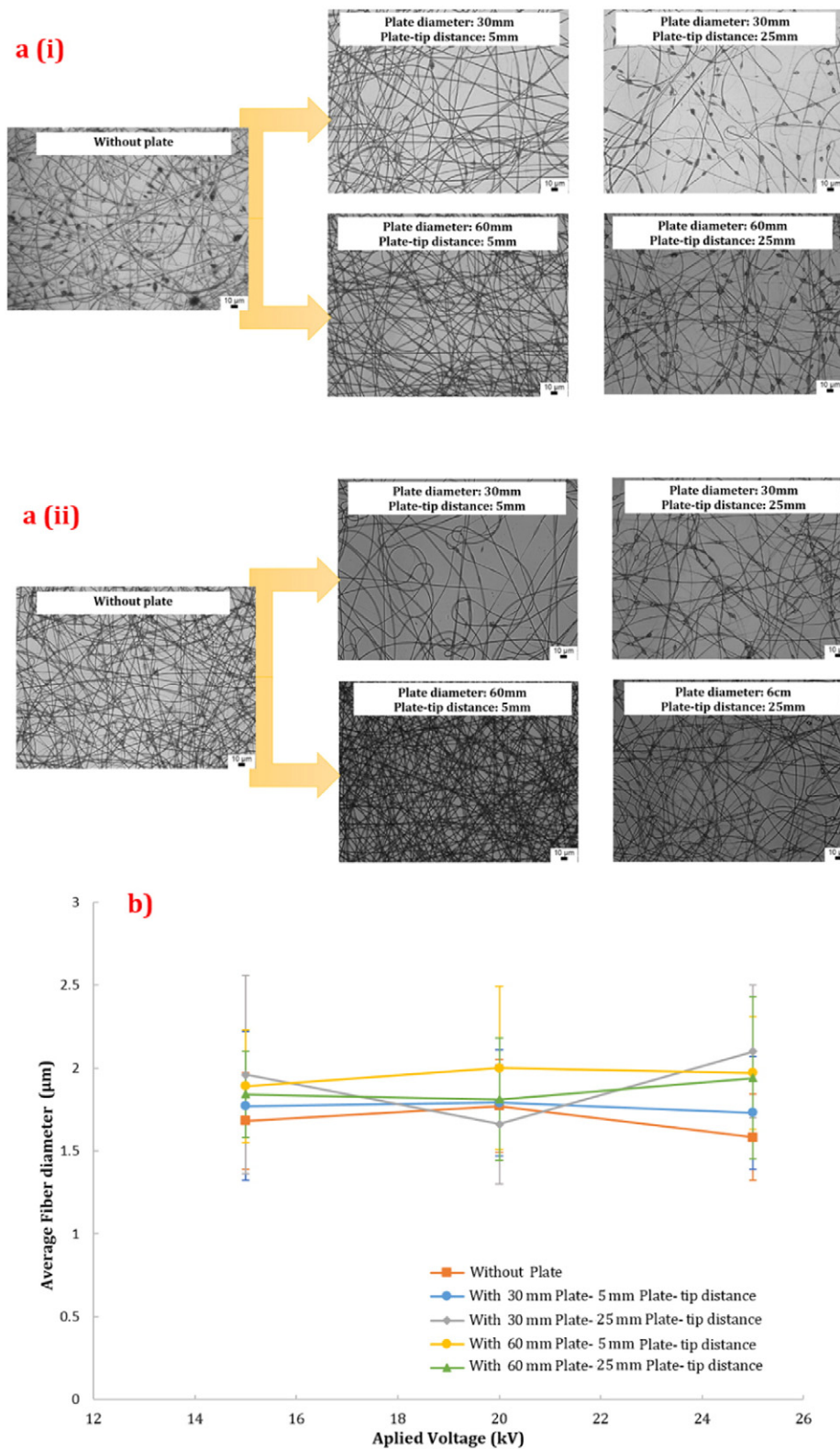
**Fig. 8.** Optical micrographs of fibres obtained from 20 wt% polymer solution at flow rate of 50 μL/min and working distance of 150 mm for applied voltages of a(i) 15 kV and a(ii) 25 kV. b) Fibre size obtained from the 20 wt% polymer solution at flow rate of 50 μL/min and working distance of 150 mm.

diameter generating larger sizes. The collection area was also observed to be concentrated in the presence of a plate, thus significantly improving the product yield. Electrospinning stability and conditions were found to be improved in the presence of a metal plate as well as on further increasing the plate diameter.

Using a plate to concentrate the electric field could be one manner to address the issue of productivity and yield of EHDA apart from other more complicated techniques used such as multi-needle electrospinning. However, further research would still be required on its applicability and feasibility for an industrial level production capacity. On a mid-market
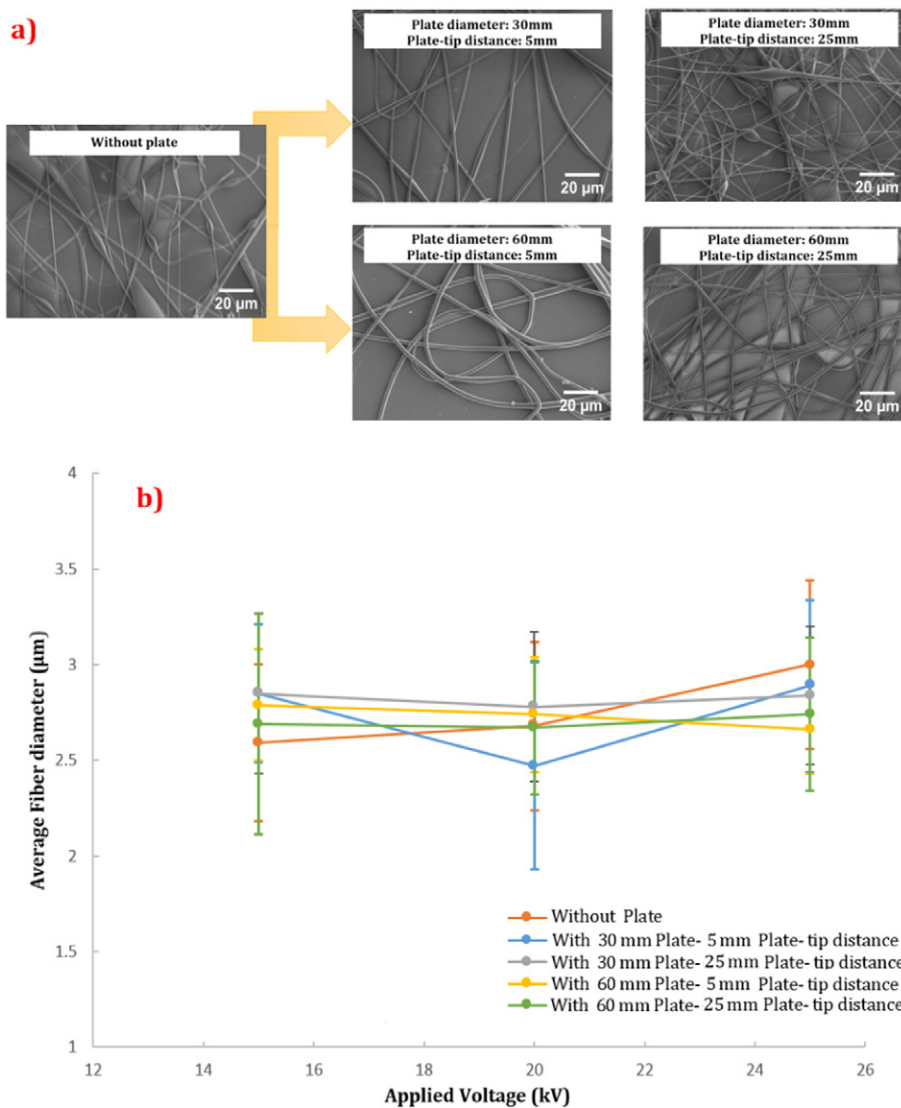
**Fig. 9.** a) Scanning electron micrographs of fibres obtained from 25 wt% polymer at flow rate of 50 μL/min and working distance of 150 mm for applied voltage of 15 kV. b) Fibre size obtained from the 25 wt% polymer solution at flow rate of 50 μL/min and working distance of 150 mm.

level, EHDA has the potential to be combined with a desktop 3D printer to cater for public consumers rather than industrial customers. The desktop 3D printing market is a huge market in itself and additionally the production level both in terms of time and cost needed for this is less demanding. This could possibly allow for better integration of EHDA systems within 3D printing through the mentioned techniques of multi-
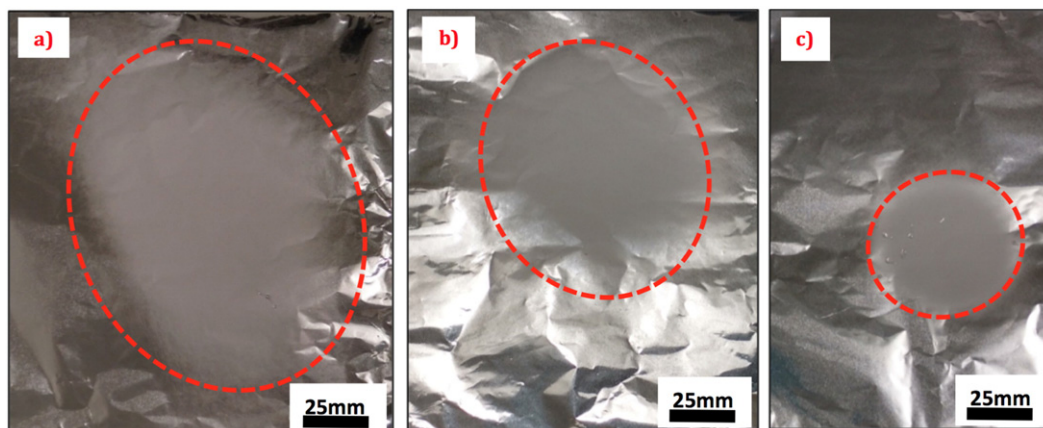


**Fig. 10.** Fibre deposition area for 25 wt% solution at flow rate 50 μL/min and working distance of 150 mm a) without the auxiliary plate, b) with 30 mm and c) 60 mm auxiliary plate.

needle electrospinning or the presence of a uniform electrical field as shown in this study.

## Acknowledgment

## References

[1] C. Luo, M. Edirisinghe, Core-liquid-induced transition from coaxial electrospray to electrospinning of low-viscosity poly (lactide-co-glycolide) sheath solution, Macromolecules 47 (2014) 7930–7938.
[2] R.A. Jain, The manufacturing techniques of various drug loaded biodegradable poly (lactide-co-glycolide)(PLGA) devices, Biomaterials 21 (2000) 2475–2490.
[3] Z. Ma, M. Kotaki, R. Inai, S. Ramakrishna, Potential of nanofiber matrix as tissue-engineering scaffolds, Tissue Eng. 11 (2005) 101–109.
[4] C. Luo, S.D. Stoyanov, E. Stride, E. Pelan, M. Edirisinghe, Electrospinning versus fibre production methods: from specifics to technological convergence, Chem. Soc. Rev. 41 (2012) 4708–4735.
[5] J. Xie, J. Jiang, P. Davoodi, M. Srinivasan, C.-H. Wang, Electrohydrodynamic atomization: a two-decade effort to produce and process micro-/nanoparticulate materials, Chem. Eng. Sci. 125 (2015) 32–57.
[6] R. Gentsch, F. Pippig, S. Schmidt, P. Cernoch, J. Polleux, H.G. Borner, Single-step electrospinning to bioactive polymer nanofibers, Macromolecules 44 (2011) 453–461.
[7] H.M. Powell, D.M. Supp, S.T. Boyce, Influence of electrospun collagen on wound contraction of engineered skin substitutes, Biomaterials 29 (2008) 834–843.
[8] M. Zamani, M.P. Prabhakaran, S. Ramakrishna, Advances in drug delivery via electrospun and electrosprayed nanomaterials, Int. J. Nanomedicine 8 (2013) 2997.
[9] Y. Wu, R.L. Clark, Electrohydrodynamic atomization: a versatile process for preparing materials for biomedical applications, J. Biomater. Sci. Polym. Ed. 19 (2008) 573–601.
[10] Y. Shin, M. Hohman, M. Brenner, G. Rutledge, Electrospinning: a whipping fluid jet generates submicron polymer fibers, Appl. Phys. Lett. 78 (2001) 1149–1151.
[11] S. Jayasinghe, M. Edirisinghe, D. Wang, Controlled deposition of nanoparticle clusters by electrohydrodynamic atomization, Nanotechnology 15 (2004) 1519.
[12] N. Bhardwaj, S.C. Kundu, Electrospinning: a fascinating fiber fabrication technique, Biotechnol. Adv. 28 (2010) 325–347.
[13] S.J. Hardman, N. Muhamad-Sarih, H.J. Riggs, R.L. Thompson, J. Rigby, W.N. Bergius, L.R. Hutchings, Electrospinning superhydrophobic fibers using surface segregating end-functionalized polymer additives, Macromolecules 44 (2011) 6461–6470.
[14] M. Lee, H.-Y. Kim, Toward nanoscale three-dimensional printing: nanowalls built of electrospun nanofibers, Langmuir 30 (2014) 1210–1214.
[15] T. Xu, K.W. Binder, M.Z. Albanna, D. Dice, W. Zhao, J.J. Yoo, A. Atala, Hybrid printing of mechanically and biologically improved constructs for cartilage tissue engineering applications, Biofabrication 5 (2013) 015001.
[16] Z. Yin, Y. Huang, N. Bu, X. Wang, Y. Xiong, Inkjet printing for flexible electronics: materials, processes and equipments, Chin. Sci. Bull. 55 (2010) 3383–3407.
[17] L. Persano, A. Camposeo, C. Tekmen, D. Pisignano, Industrial upscaling of electrospinning and applications of polymer nanofibers: a review, Macromol. Mater. Eng. 298 (2013) 504–520.
[18] M. Richard-Lacroix, C. Pellerin, Molecular orientation in electrospun fibers: from mats to single fibers, Macromolecules 46 (2013) 9473–9493.
[19] P. Gupta, C. Elkins, T.E. Long, G.L. Wilkes, Electrospinning of linear homopolymers of poly (methyl methacrylate): exploring relationships between fiber formation, viscosity, molecular weight and concentration in a good solvent, Polymer 46 (2005) 4799–4810.
[20] B. Veleirinho, M.F. Rei, J. Lopes-DA-Silva, Solvent and concentration effects on the properties of electrospun poly (ethylene terephthalate) nanofiber mats, J. Polym. Sci. B Polym. Phys. 46 (2008) 460–471.
[21] P.-D. Hong, C.-M. Chou, C.-H. He, Solvent effects on aggregation behavior of polyvinyl alcohol solutions, Polymer 42 (2001) 6105–6112.
[22] J. Deitzel, J. Kleinmeyer, D. Harris, N.B. Tan, The effect of processing variables on the morphology of electrospun nanofibers and textiles, Polymer 42 (2001) 261–272.
[23] H. Fong, I. Chun, D. Reneker, Beaded nanofibers formed during electrospinning, Polymer 40 (1999) 4585–4592.
[24] C.-M. Hsu, S. Shivkumar, Nano-sized beads and porous fiber constructs of poly (ε-caprolactone) produced by electrospinning, J. Mater. Sci. 39 (2004) 3003–3013.
[25] A. Bohr, M. Yang, S. Baldursdóttir, J. Kristensen, M. Dyas, E. Stride, M. Edirisinghe, Particle formation and characteristics of Celecoxib-loaded poly (lactic-co-glycolic acid) microparticles prepared in different solvents using electrospraying, Polymer 53 (2012) 3220–3229.
[26] K. Nasouri, A. Haji, A. Shoushtari, A. Kaflou, A Novel Study of Electrospun Nanofibers499 Morphology as a Function of Polymer Solution Properties, Proc. Int. Conf. Nanomaterials Applications and Properties 2 (3) (2013) 03NCNN04-1(4pp).
[27] C.M. Hsu, S. Shivkumar, N, N-dimethylformamide additions to the solution for the electrospinning of poly (ε-caprolactone) nanofibers, Macromol. Mater. Eng. 289 (2004) 334–340.
[28] A. Koski, K. Yim, S. Shivkumar, Effect of molecular weight on fibrous PVA produced by electrospinning, Mater. Lett. 58 (2004) 493–497.
[29] I. Hayati, A. Bailey, T.F. Tadros, Investigations into the mechanism of electrohydrodynamic spraying of liquids: II. Mechanism of stable jet formation and electrical forces acting on a liquid cone, J. Colloid Interface Sci. 117 (1987) 222–230.
[30] S. Chakraborty, I.-C. Liao, A. Adler, K.W. Leong, Electrohydrodynamics: a facile technique to fabricate drug delivery systems, Adv. Drug Deliv. Rev. 61 (2009) 1043–1054.
[31] K. Garg, G.L. Bowlin, Electrospinning jets and nanofibrous structures, Biomicrofluidics 5 (2011) 013403.
[32] C. Thompson, G. Chase, A. Yarin, D. Reneker, Effects of parameters on nanofiber diameter determined from electrospinning model, Polymer 48 (2007) 6913–6922.
[33] Y. Yang, Z. Jia, J. Liu, Q. Li, L. Hou, L. Wang, Z. Guan, Effect of electric field distribution uniformity on electrospinning, J. Appl. Phys. 103 (2008) 104307.
[34] S. Xie, Y. Zeng, Effects of electric field on multineedle electrospinning: experiment and simulation study, Ind. Eng. Chem. Res. 51 (2012) 5336–5345.
[35] S. Agarwal, J.H. Wendorff, A. Greiner, Progress in the field of electrospinning for tissue engineering applications, Adv. Mater. 21 (2009) 3343–3351.

**O. Husain** graduated with a Bachelor in Mechanical Engineering from the University of Sheffield, UK, in 2014. He recently completed his M.Sc degree in Engineering with Finance at the University College London, UK.

**W. Lau** obtained a degree in Biomedical Science from King's College London and a Masters in Biomaterials and Tissue Engineering at University College London for which he obtained a distinction and was mentioned on the Dean's list of commendations. He was awarded funding by the EPSRC and the IBME at UCL to undertake his PhD in Prof. Edirisinghe's laboratory. His current research topic investigates novel methods of utilising electrohydrodynamic processing for biomedical applications. He is currently under the employment of AtoCap Ltd. to spearhead the development of co-axial electrospraying technology for industry.

**M. Edirisinghe** has pioneered both fundamental and user-inspired engineering research, leading to remarkable progress and international excellence in the novel forming of advanced materials. He has invented many processes and devices for the preparation of bubbles, vesicles, particles, capsules and fibres and has been awarded numerous prizes, including the Royal Society Brian Mercer Feasibility Award for an unprecedented three times. His seminal work has resulted in significantly advancing areas crucial to the betterment of life, such as optimal drug delivery, smart orthopaedic coatings and the translation of novel medical technologies from the laboratory to clinical practice.

**M. Parhizkar** studied Mechanical Engineering at Brunel University and achieved a MEng degree in 2007. She joined Jacobs Engineering in 2008 as a junior consultant, working on a number of engineering and design projects. In 2010, she started her PhD degree in Prof. Edirisinghe's lab at University College London. Her research focus was production of microbubbles/scaffold using microfluidics and electrohydrodynamic techniques. Since 2014, she has been working as a post-doctoral research associate on a EPSRC funded project investigating new methods of delivery of Cisplatin utilising particles and microbubbles.